Journal of the European Ceramic Society 21 (2001) 343–354

www.elsevier.com/locate/jeurceramsoc

Reaction sintering of zircon–dolomite mixtures

J.L. Rodríguez [a,1], M.A. Rodríguez [b], S. De Aza [b], P. Pena [b,*]

[a] *CINVESTAV-IPN, Carr. Saltillo Coah., Mexico*
[b] *Instituto de Cerámica y Vidrio, CSIC, 28500 Arganda del Rey, Madrid, Spain*

Received 16 March 2000; received in revised form 7 July 2000; accepted 15 July 2000

Abstract

Dolomite–zircon mixtures have become interesting for finding alternate sources to improve the production of high magnesia refractories. To asses this option, two minerals, dolomite and zircon were selected, as economically raw materials, to produce $MgO–CaZrO_3–Ca_2SiO_4$ materials. The reaction sintering mechanism of zircon–dolomite mixtures were investigated using finely ground Spanish dolomite and zircon powders as starting materials. During the heat treatment decomposed dolomite ($CaO + MgO$) reacts with zircon, from 1000 to 1200°C, through a series of reactions before the final stable compounds are formed. From the results obtained the reaction occurs prior to sintering in the presence of an amorphous transitory phase, magnesium calcium silicate phase and the limiting process during the reaction is the formation of Ca_2SiO_4. The sintering occurs after the end of the reaction so by controlling the whole process it is possible to obtain materials with controlled porosity. In the present work it is shown that reaction sintering of zircon–dolomite mixtures is a feasible route to obtain $MgO–CaZrO_3–\beta$-Ca_2SiO_4 porous materials for refractory insulators or as filters applications.

Keywords: Dolomite; MgO; Microstructure-final; Reaction sintering; Refractories; Zircon

1. Introduction

Silicate-bonded magnesia materials have a high thermal expansion coefficient coupled with poor thermal spalling resistance. When they are combined with chromium or aluminium oxide, thermal shock resistance and other properties are improved. When X_2O_3 ($X = Cr^{3+}$, Al^{3+}) addition is higher than 15% secondary phase bridges of spinel between MgO grains are formed i.e. ($Cr_2O_3 + MgO \rightarrow MgCr_2O_4$). These bridges give ''direct bonding'' i.e. solid–solid bonds of MgO–spinel phase or spinel–spinel.[1,2]

Environmental protection regulations[3] (ban of magnesia chrome based raw materials) led to the development of new phase-bonded magnesia materials with similar or improved high temperature mechanical properties. A new processing route consists in adding zircon in order to form $CaZrO_3$ bonded materials. The thermal expansion of $CaZrO_3$ (7.0×10^{-6} C^{-1} from 20 to 1000°C)[4] and Ca_2SiO_4 (4.0×10^{-6} C^{-1} from 20 to 1000°C) compared to MgO (13.5×10^{-6} C^{-1}) can lead to the formation of gaps between Ca_2SiO_4, $CaZrO_3$ and MgO grains. These discontinuities can increase toughness and thermal shock resistance by stopping crack propagation.

Dicalcium silicate (Ca_2SiO_4) has five polymorphs, among which the (β) orthorhombic to (γ) monoclinic transformation is similar to the tetragonal to monoclinic transformation in ZrO_2, in that they both experience a volume increase on transformation during cooling.[5] However, differences exist between these two corresponding transformations. Firstly, in Ca_2SiO_4 the transformation occurs from a twinning β microstructure to an untwinned γ structure, while in ZrO_2 the reverse is true. Secondly, unlike ZrO_2, the transformation from β to γ is irreversible, since β is a metastable phase. Thirdly, the volume increase associated with the phase transformation is 12% for Ca_2SiO_4, while it is only 4.9% for ZrO_2, both at room temperature.

To assess this option, two minerals, dolomite ($MgCa(CO_3)_2$) and zircon ($ZrSiO_4$) were selected to produce $MgO–CaZrO_3–Ca_2SiO_4$ materials according to the reaction:

* Corresponding author.
E-mail address: ppena@icv.csic.es (P. Pena).
[1] Present address: Instruto de Ceramica y Vidrio, CSIC.

0955-2219/01/$ - see front matter
PII: S0955-2219(00)00212-0

$$ZrSiO_4 + 3\ MgCa(CO_3)_2 \rightarrow 3MgO + CaZrO_3 + \beta\text{-}Ca_2SiO_4 + 6\ CO_{2(g)} \quad (1)$$

The use of naturally minerals is an attractive alternative for the production of low cost, MgO-based, high temperature structural materials. Naturally occurring minerals with consistent chemical composition, dolomite and zircon, were selected as economically interesting reactants. Europe is one area with significant deposits of high quality dolomite and in the south of Spain there are important quarries of dolomite with very high quality.

In order to elucidate on the reaction sintering mechanism between dolomite and zircon and the viability of this method, the reaction sintering of a homogeneous mixture of dolomite–zircon powders has been studied. The reaction sintering process has been explored using constant heating rate dilatometry and thermal analysis (DTA-TG) in the homogeneous mixture. The reactions involved and the final phase mineral constitution

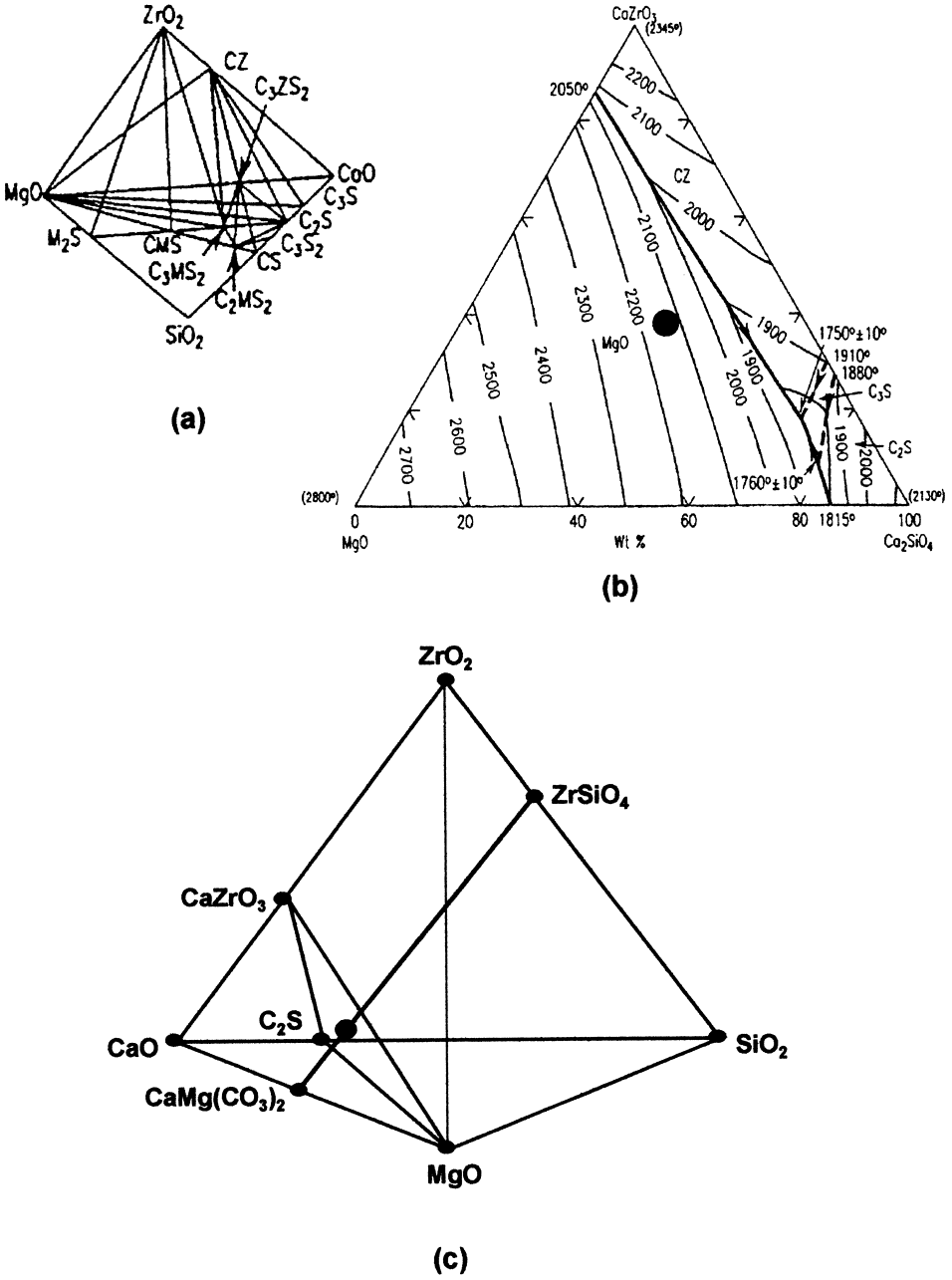

Fig. 1. Phase diagram of the MgO–CaO–ZrO_2–SiO_2 system: (a) solid state compatibility relationships; (b) phase diagram of the section MgO–$CaZrO_3$–Ca_2SiO_4 showing phase boundaries and isotherms on the liquidus surface; (c) diagrammatic representation of the intersection between the solid state compatibility MgO–$CaZrO_3$–Ca_2SiO_4 plane and the dolomite–zircon formulation line.

was characterised by X-ray diffraction (XRD) and scanning electron microscopy (SEM–EDX).

2. Experimental procedures

The raw materials used in this work were zircon (Zircosil, Cookson Ltd) and a finely milled mineral dolomite supplied by Prodomasa, Spain. Chemical analyses of both raw materials were done by inductively coupled plasma spectrometry (ICP), atomic absorption spectrometry (ASS), and gravimetry analysis. The $ZrSiO_4$/$MgCa(CO_3)_2$ composition was prepared according to the stoichiometry proportion of Eq. (1). This composition was formulated on the basis of the information supplied by the quaternary system CaO–MgO–ZrO_2–SiO_2. In Fig. 1(a) the phase diagram of the section MgO–$CaZrO_3$–Ca_2SiO_4 and a diagrammatic representation of the solid state relationships are shown.[6,7] The studied composition lie in the solid-state compatibility plane MgO–$CaZrO_3$–Ca_2SiO_4 and are located in the straight-line zircon–dolomite Fig. 1(b). From the section MgO–$CaZrO_3$–Ca_2SiO_4 it can be stated that the composition considered is located in the primary field of MgO and the secondary phase is $CaZrO_3$. According to the quaternary system, for this composition, the initial liquid formation starts at 1750°C invariant point of the subsystem MgO–$CaZrO_3$–Ca_2SiO_4.

Dolomite–zircon *stoichiometric mixture* was homogenised by attrition milling in water media. The surface area of the homogenised powders was measured by the N_2 gas adsorption method using the BET single point procedure (Quantachrome, Monosorb model) and the grain size distribution was determined in a laser scattering apparatus (Malvern, Mastersizer S, UK). After spray drying bars, of about 5 mm diameter, were made by using a cold isostatic press (National Forge, Belgium) under 200 MPa.

DTA-TGA (STA 409, Netzch, Germany) studies were conducted on cold isostatically pressed compacts, in air, using Pt crucibles. Thermal shrinkage curves were carried out on similar compacts. A dilatometer LVDT was used (Geratebav GmbH Dil-402 E/7, Neztch, Germany). The thermal studies were performed up to 1500°C and at a constant heating rate of 2°C min^{-1}.

The specimens were fired in a high temperature electric furnace at temperatures in the range of 800–1740°C. The heating rate was 2°C min^{-1} up to final temperature and samples remained 2 h at this level. Fired products thus obtained were characterised in terms of bulk density, microstructure and phase composition. Bulk density and porosity of the green and sintered products were determined by liquid displacement using Archimedes principle in Hg and by Hg-porosimetry (Micromeritics

Table 1
Physical characteristics and chemical analysis of the raw materials

	Zircon	Dolomite
Chemical analysis:		
Ignition loss	1.02%	47.8%
CaO	0.1 (by ICP-plasma)	30.8 (by gravimetry)
MgO	0.02 (by ICP-plasma)	22.1 (by gravimetry)
ZrO_2 (by ICP-plasma)	62.3	n.d.
HfO_2(by ICP-plasma)	1.20	–
Y_2O_3(by ICP-plasma)	0.11	–
SiO_2 (by ICP plasma)	34.6	0.17
Al_2O_3 (by ICP-plasma)	0.03	0.011
Fe_2O_3 (by ICP-plasma)	0.02	0.001
MnO (by ICP-plasma)	n.d.	0.001
Nb_2O_5 (by ICP-plasma)	n.d.	0.0004
TiO_2 (by ICP-plasma)	0.07	0.001
P_2O_5 (by ICP-plasma)	n.d.	0.001
SrO (by ICP-plasma)	n.d.	0.006
Na_2O (flame photometry)	0.006	0.005
K_2O (flame photometry)	n.d.	0.002
Physical properties		
Specific surface BET (m^2 g^{-1})	12	2.5
Particle size (μm)	1.1	4.5

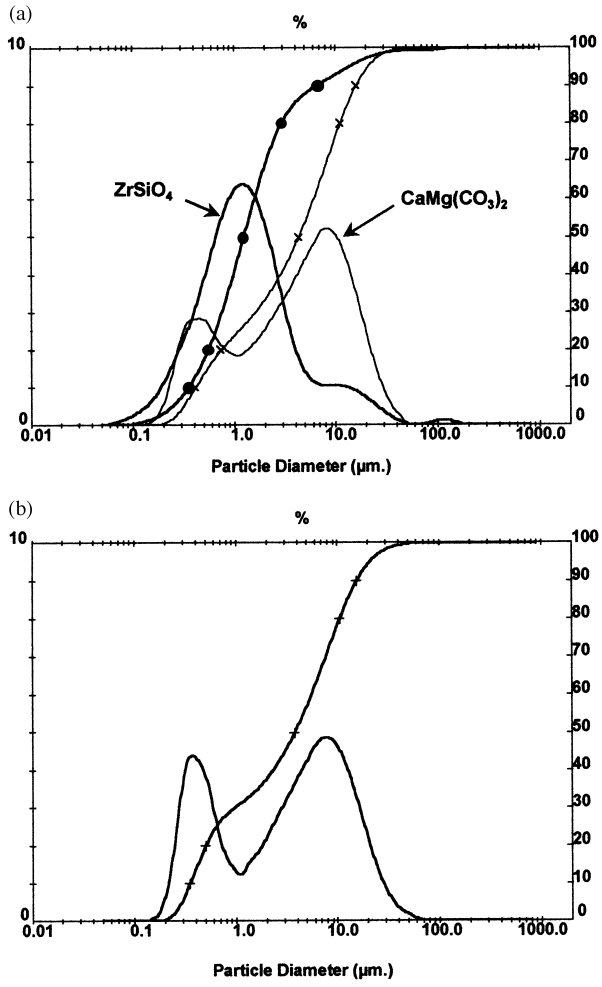

Fig. 2. (a) Particle size distribution of $CaMg(CO\cdot)_2$ and $ZrSiO_4$ raw materials; (b) particle size distribution of the S1 sample.

Autopore) respectively. X-ray powder diffraction patterns of the raw and fired materials obtained using a diffractometer (model Kristalloflex D-5000, Siemens, Germany) with nickel filtered Cu-K_α radiation operating at 50 kV and 30 mA. Diffraction patterns were recorded from the 2θ range 10–70°. Microstructural analysis and phase identification were done by reflected light microscopy (Carl Zeiss D-7082, Oberkochen, Germany) and scanning electron microscopy (Zeiss DMS 950, Germany) with energy dispersive X-ray analyser using sputtered gold coating on both fractured and polished thermally etched surfaces of the sintered samples. The grain size average was determined by the line intersection method.[8]

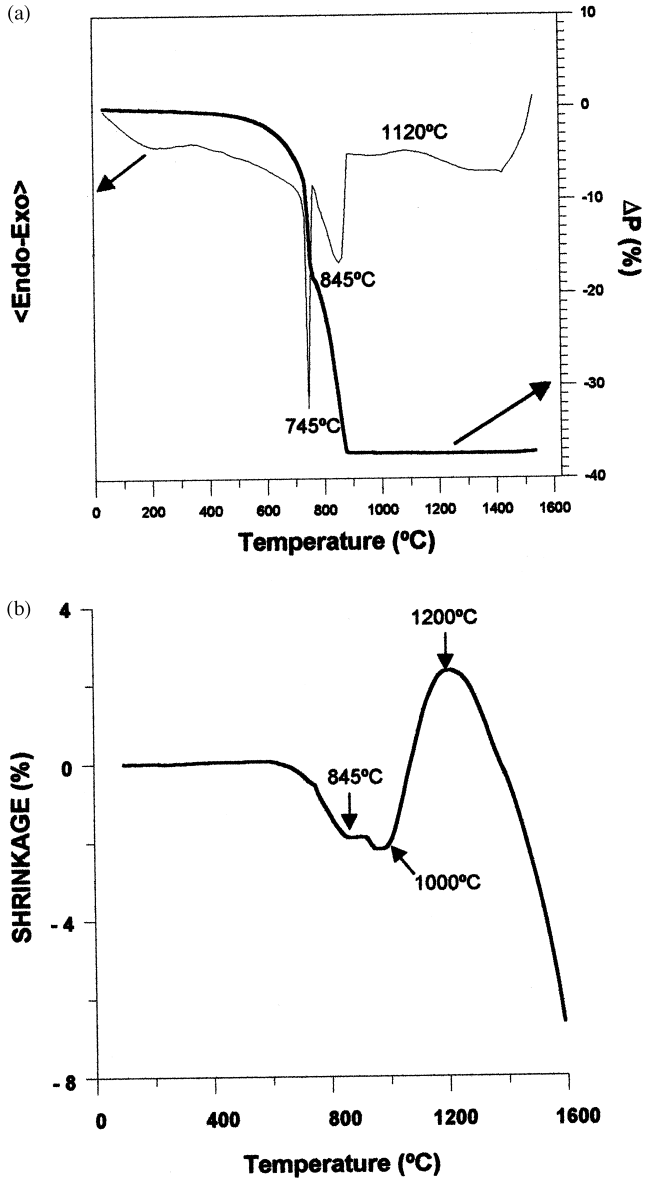

Fig. 3. Thermal behaviour of green compacted samples at a heating rate 2°C/min: (a) differential thermal analysis plot (DTA) and thermogravimetric analysis (TG); (b) constant heating rate dilatometry curve (CHRD).

3. Results

The physico-chemical characteristics of dolomite and zircon are given in Table 1. The natural Spanish dolomite powder was white and contrary to other dolomite minerals this specimen contains negligible amounts of iron and manganese. There was very little impurity <0.03 wt.%, and the CaO/MgO molar ratio of dolomite was almost identical with the theoretical value ($CaO/MgO = 1.002$). The silica content of the zircon powder is higher than the stoichiometric amount ($ZrO_2 + HfO_2/SiO_2 = 0.888$). There was little impurity of aluminium oxide also.

Powder X-ray diffraction analysis clearly indicates that the powders consists of pure well crystallised dolomite and zircon respectively in good agreement with chemical analyses.

The grain size distribution measured by laser scattering granulometry of dolomite, zircon and the composition studied, S1, are shown in Fig. 2 (a) and (b). Dolomite powders present a coarse granulometry with a medium average particle size of 4.5 μm. It is worth to say that a 10% of dolomite particles have a grain size between 16 and 50 μm. The medium average grain size of zircon

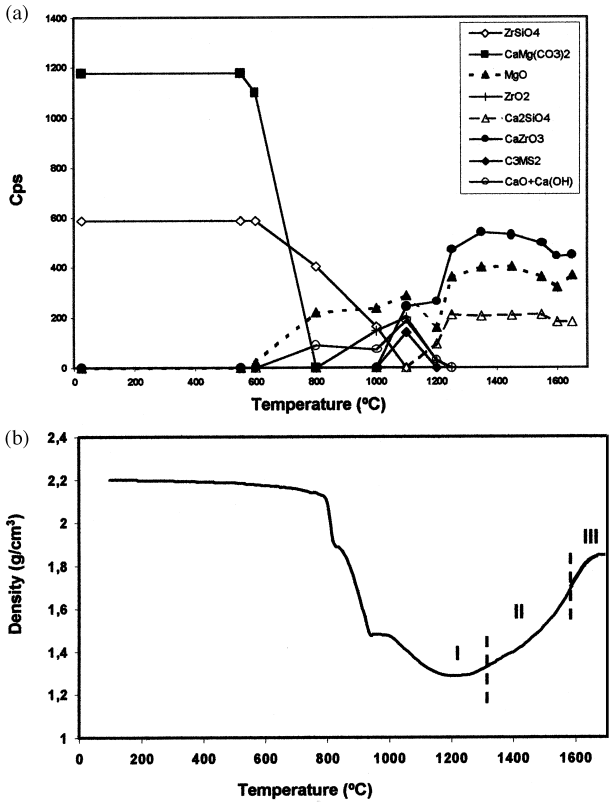

Fig. 4. (a) Phase composition — heat treatment temperature plots as indicated from the following XRD peaks: $CaMg(CO_3)_2$ (104); $ZrSiO_4$ (200); MgO (200), t-ZrO_2 (101); $CaZrO_3$ (121); $Ca_3MgSi_2O_8$ (013), Ca_2SiO_4 (−121), $CaO + Ca(OH)_2$ (200) and (001) respectively; (b) bulk density of the sample versus sintering temperature. I indicates initial stage of sintering, II intermediate and III final.

was located at 1.2 μm. Zircon powders present a small amount of soft agglomerates with sizes between 6 and 40 μm. The grain size distribution of the studied sample, homogenised dolomite–zircon powders, Fig 2b, shows a bimodal behaviour, with a component centred at 0.35 μm and the second one at 8 μm. Bearing in mind the data of dolomite and zircon powders the coarse fraction of the mixture would be fundamentally constituted by dolomite and the finest fraction would correspond to zircon. After homogenisation approximately 10% of particles have again grain sizes between 16 and 50 μm. The specific surface of the studied powder mixture was 2.4 m^2/g.

The porosity of green bars after isostatic pressing at 200 MPa was 25% and the average pore size was 0.24 μm.

3.1. Dynamic sintering studies

When the cold isostatic pressed compact of dolomite–zircon mixture is subjected to thermal treatment at a constant heating rate, several phenomena are observed. In Fig. 3 (a) and (b), the thermal and dilatometric events identified by the temperature are:

1. In TG, a weight loss of 37 wt.% was observed. At 745 and 845°C DTA curve exhibited two endothermic peaks, characteristics of decarbonation of dolomite at low CO_2 pressure (atmospheric pressure) Otsuka[9] and De Aza et al.[10]

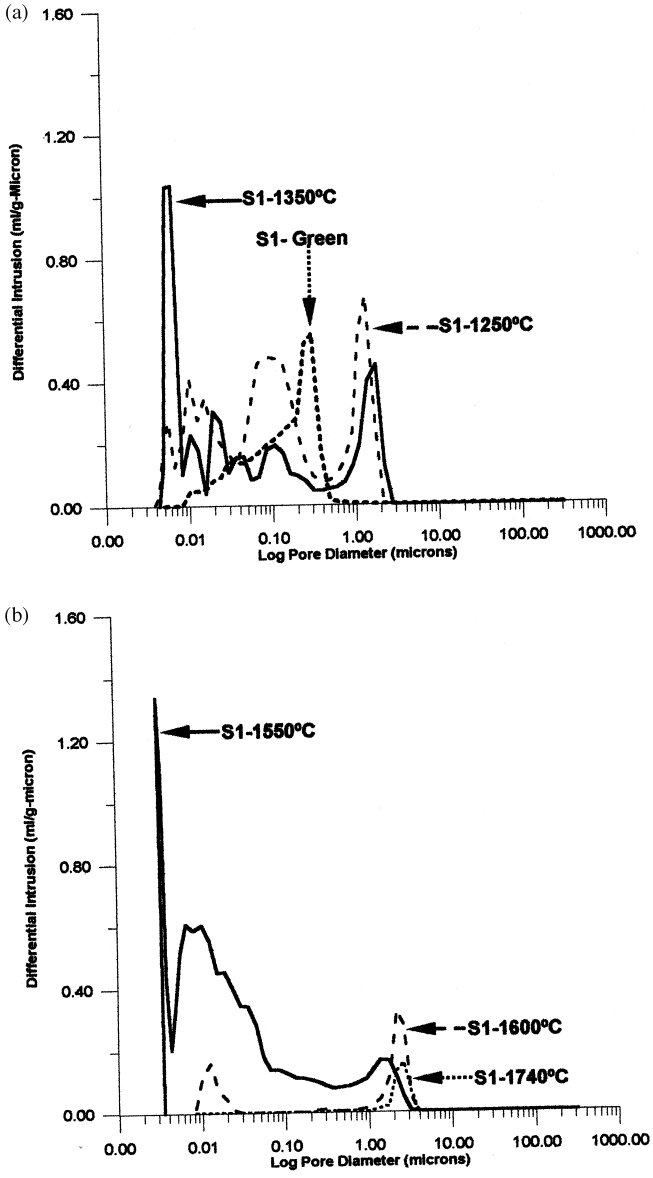

Fig. 5. Pores size distribution of S1 compacts heated at different temperatures for 2 h: (a) green, 1250 and 1350°C; (b) 1550, 1600 and 1740°C.

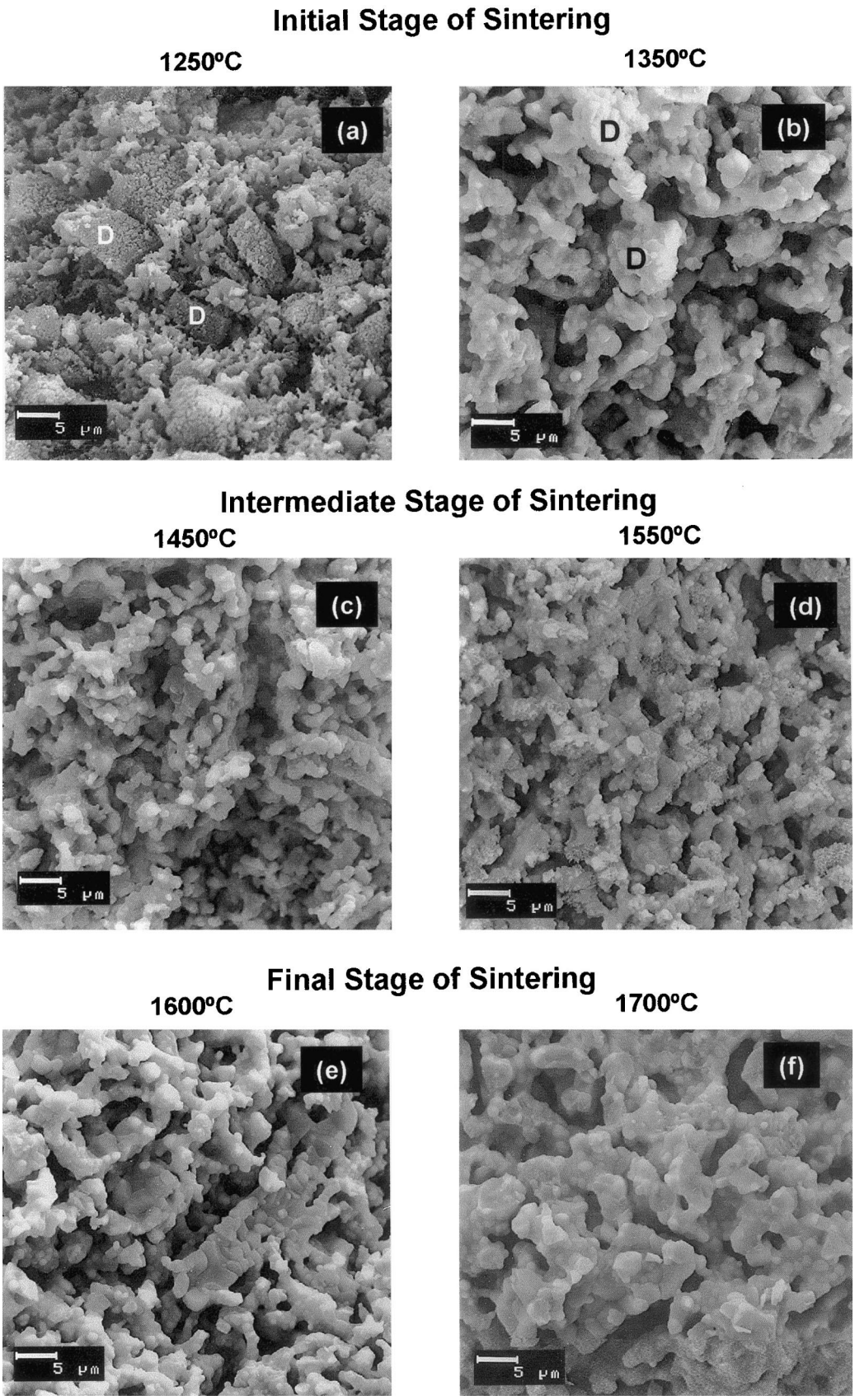

Fig. 6. Microstructural evolution of the sample with temperature as observed by back scattered SEM on fractured surfaces of samples sintered for 2 h at: (a) 1250°C; (b) 1350°C; (c) 1450°C (d) 1550°C (e) 1600°C and (f) 1700°C. Label D corresponds to dolomite aggregates.

$$CaMg(CO_3)_2\ (s) \rightarrow Ca_{1-x}Mg_xCO_3\ (s) + MgO\ (s) + CO_{2(g)} \quad (2)$$

$$CaCO_{3(s)} \rightarrow CaO_{(s)} + CO_{2(g)} \quad (3)$$

The slight shrinkage of the compact in the range to 745–845°C can be attributed with the weight losses associated to the dolomite decomposition. The expansive effect at 845°C is attributed to the decomposition of $CaCO_3$.

2. Above 900°C CaO and MgO react with zircon, and a broad exothermic peak is noticed with a maximum at 1120°C and expansive effect at 1000°C in the dynamic sintering curve (CHR).
3. At temperatures higher than 1250°C a significant shrinkage can be observed.

In order to determine the reaction sintering sequence, green compacted samples were heated at temperatures ranging from 1200 to 1740°C for 2 h.

The evolution of the reaction sintering process has been studied by X-ray diffraction in the mentioned samples. In Fig. 4(a) the semi-quantitative XRD analysis of the reaction process is shown. From these curves the reaction is practically finished (≈95%) at 1250°C. XRD patterns of the zircon–dolomite mixture treated at temperatures higher than 1250°C revealed the presence of three main phases MgO (periclase), $CaZrO_3$ and β-Ca_2SiO_4. At 1000°C by XRD $ZrSiO_4$, MgO, $Ca(OH)_2$ + CaO, t-ZrO_2 and a meta-stable amorphous phase can be detected. The compact treated at 1100°C shown the phases MgO, $Ca(OH)_2$ + CaO, t-ZrO_2, $CaZrO_3$, $Ca_3Mg(SiO_4)_2$ and an amorphous phase revealed by the broad peak at low angles. As is well known, CaO easily reacts with moisture in air to form $Ca(OH)_2$, hence its presence in XRD patterns.

Samples heated in the range of temperatures 800–1000°C showed pronounced macroscopic cracking over the whole sample. These samples are not stable in air because in a short period of time the hydration of the free lime disaggregates the sample. By this reason it was not possible to get stable materials in this interval of temperatures.

The densification behaviour of the compacted green sample calculated from termogravimetric and dilatometric analysis is shown in Fig. 4(b). Density at each temperature is given by Eq. (4):

$$\rho_t = \frac{P_t}{l_t^3} = \frac{P_0(1+\Delta P)}{[l_0(1+\Delta l)]^3} = \rho_0 \frac{(1+\Delta P)}{(1+\Delta l)^3} + \frac{\rho_0 \bullet \Delta P}{(1+\Delta l)^3} \quad (4)$$

where ρ_0 = is the green density of the compact, ΔP weight loss and Δl = shrinkage data.

According to Fig. 4 in this process the chemical reaction and the densification of the compact takes place in two well-differentiated steps. Chemical reaction of reactants is practically completed at 1250°C whereas at this temperature porosity is much higher (61%) than the initial (25%). Reaction between zircon and dolomite occurs with significant changes in volume and loss of CO_2, 37 wt.%.

3.2. Microstructural static study of sintering

Samples heated 2 h at temperatures higher than 1250°C were studied by Hg-porosimetry and scanning

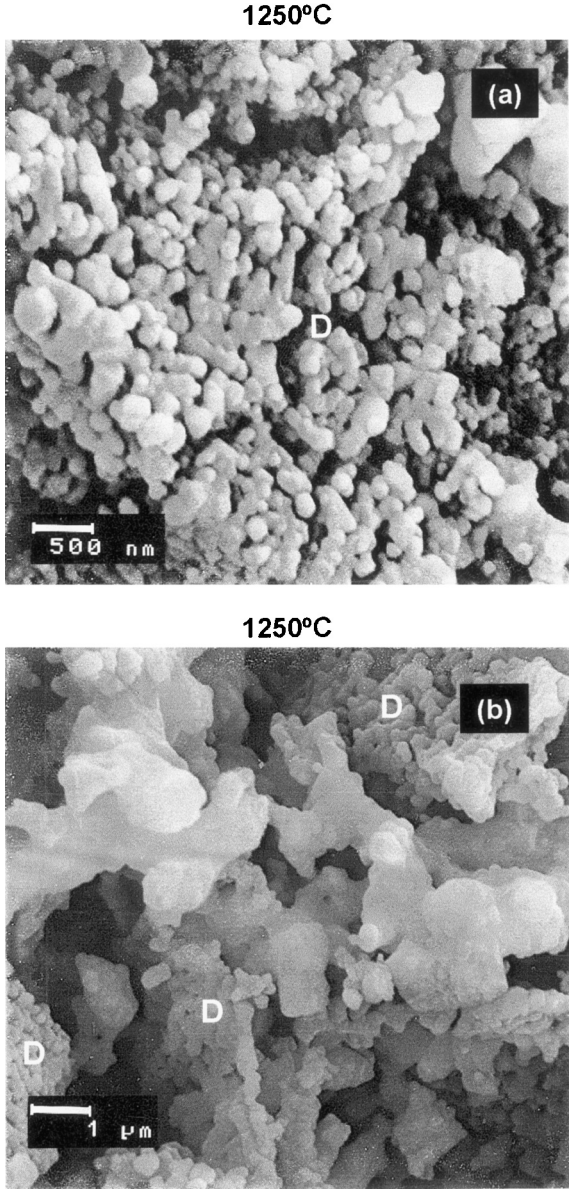

Fig. 7. Back scattered electron microscopy images of fractured surfaces of sample heat-treated for 2 h showing the initial stage of sintering. General view and detail of sample sintered at 1250°C showing decomposed dolomite agglomerates and neck formation: (a) detail of dolomite aggregates; (b) detail of fine fraction of sample.

electron microscopy in order to clarify the sintering mechanism.

Hg porosimetry results are shown in Fig. 5. It can be observed how the porosity size growths from green material up to 1250°C. Thermal treatment between 1250 and 1550°C decreases pore size due to the sintering of the particles. At higher temperatures pore size increased by porous coalescence.

Fig. 6 shows back-scattered electron microscopy images of fractured surfaces of the sample heated between 1250 and 1700°C. The reaction processes disrupts the initial microstructure and the porous network formed makes difficult the densification process of the new microstructure. At temperatures as high as 1600°C the porosity of the sample is still 55%.

In Fig. 6(a) clusters of MgO + CaO formed from the small quantity of dolomite particles with a grain size larger than 20 μm can clearly be distinguished. Gaps between these clusters and the finest fraction of the sample are detected and no neck formation between these particles can be seen. Fig. 7(a) shows a high magnification of decomposed coarse dolomite grains showing porous microstructures formed by homogeneously distributed CaO and MgO particles with an average particle size of ≈100 nm; neck formation between these nanosized particles is clearly observed. In Fig. 7(b) corresponding to the finest fractions of the compact, neck formation between particles can also be observed.

In samples treated at 1350°C, Fig. 6(b), dolomite aggregates show significant sinterization, inter-granular fracture and considerable increment in grain and pore size. The grain size at this temperature is within the range from 700 nm to 2 μm. The neck formation between particles is evident too at low magnifications.

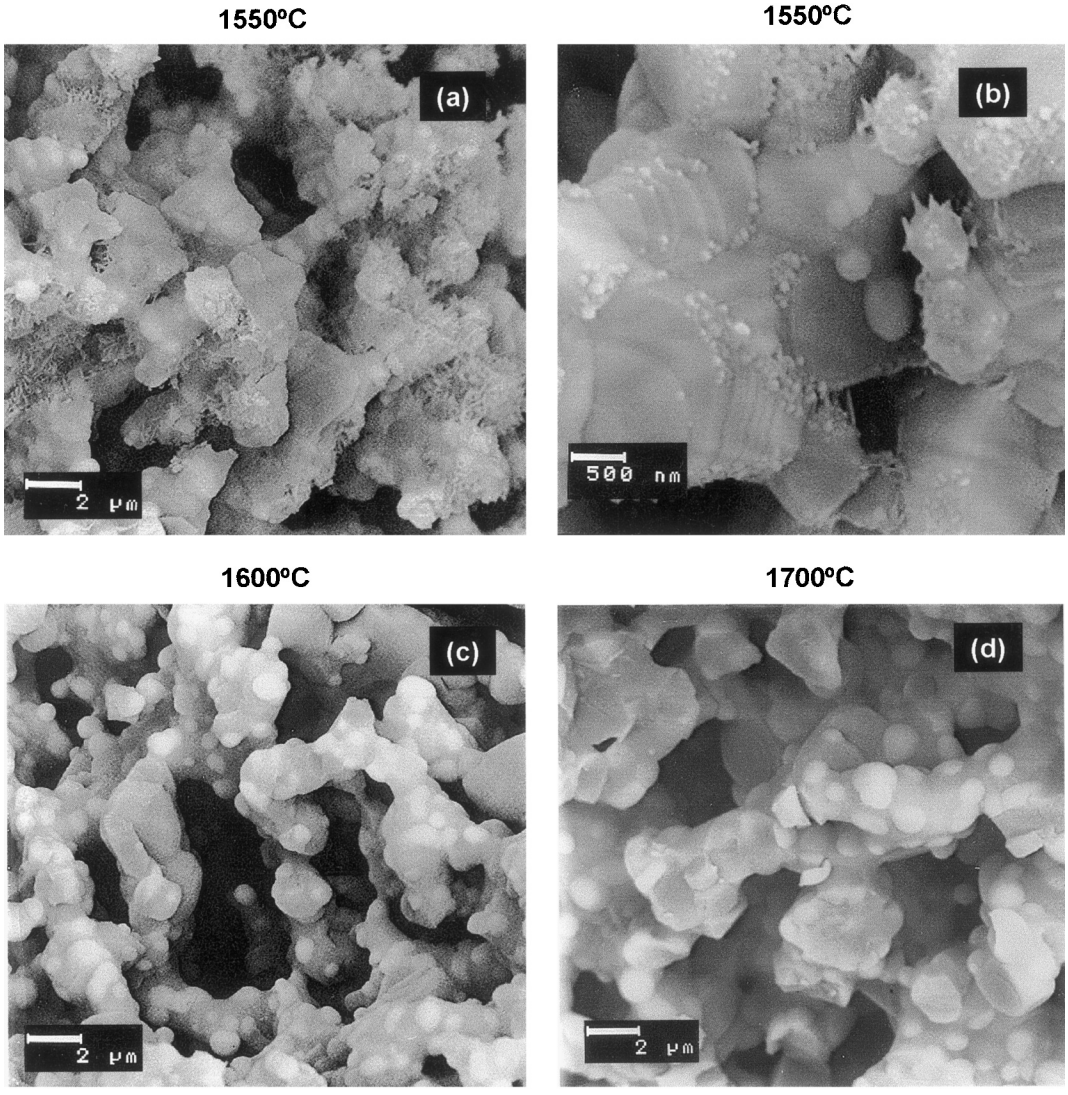

Fig. 8. Back scattered electron microscopy images of fractured surfaces of sample heat-treated for 2 h showing the intermediate stage of sintering: (a) and (b): general view and detail of sample sintered at 1550°C showing needless and droplets of the transitory liquid phase formed; (c) and (d) general view of samples sintered at 1600 and 1700°C respectively.

At 1450°C, Fig. 6(c), the initial formation of pore channels by coalescing the small ones is observed but no significant grain growth is detected.

At 1550°C, Figs. 6(d) and 8(a) and (b), the formation of nanometric needles and droplets, in pore surface, suggests the formation of very small quantities of transitory liquid and crystalline phases.

At 1600°C, the mentioned transitory phases are not detected [see Figs. 6(e) and 8(e)]. Inter-connected porosity increases and a significant grain growth begins. At 1700°C, Figs 6(f) and 8(d), the channel and interconnected porosity increases. Polished and thermally etched surfaces of the sample heat treated at 1740°C were studied by SEM-EDX. After densification at 1740°C porosity remained as high as 40% and limited grain growth was observed. The more significant microstructural features of the sample can be observed in Figs. 9 and 10.

Fig. 9(a) shows a typical back-scattered microstructure of sample in which porous channels with 1–2 μm diameter, porous segregations and densified areas can be identified. Fig. 9(b) shows a microstructural detail of dense areas of Fig. 9(a), in this microphotography the three main types of crystalline phases can be identified: periclase (MgO), calcium zirconate ($CaZrO_3$) and dicalcium silicate (Ca_2SiO_4).

Chemical and microstructural segregations identified during the microstructural study can be classified in two types of defects: (a) clusters of CaO and MgO particles (30–40 μm) and (b) $CaZrO_3/Ca_2SiO_4$ agglomerates (20–60 μm).

The porous clusters, formed by a microporous homogeneous mixture of CaO and MgO particles (1–2 μm) surrounded by channels of pores, can be observed with their corresponding microanalysis in Fig. 10(a). This kind of clusters was also observed in the samples treated at lower temperatures; 1250 and 1350°C (Figs. 6 and 7). Heterogeneous $CaZrO_3/Ca_2SiO_4$ clusters (30–60 μm) surrounded by a big pore with are detected. An example of the constitution of these clusters can be seen in Fig. 10(b). In it, there are agglomerates of $CaZrO_3$ grains, 2–3 μm, surrounded by a big pore in one side and by a layer of big Ca_2SiO_4 grains, 10 μm, in the other one. The Ca_2SiO_4 grains presented small $CaZrO_3$ grains inside and between the grain boundaries. Also small quantities of glassy phase at the grain boundaries were observed. Reaction between zircon agglomerates and the small fraction of dolomite grains formed this second type of defects. These clusters were in equilibrium at local level and were not possible to eliminate by heat treatment.

4. Discussion

In the densification of reacting powder systems two phenomena occur: porosity removal and reaction. Consequently the control of the rate at which each of these phenomena take place is the first stage to achieve the desired microstructures and properties of reaction sintering materials.

The studied reaction process occurs with a weight loss of CO_2, 37 wt.%, at temperatures higher than 700°C just as it is observed in Fig. 3(a). During the heat treatment dolomite decomposes in two steps according to reactions (2) and (3); decomposed dolomite (CaO + MgO) reacts with zircon between 1000 and 1200°C and goes through the next reactions:

$$\{CaO + MgO\} + ZrSiO_4 \rightarrow Ca_3Mg(SiO_4)_2 + t\text{-}ZrO_2 + MgO + \text{amorphous phase} \quad (5)$$

$$t\text{-}ZrO_2 + \text{amorphous phases} \rightarrow CaZrO_3 + \text{amorphous phase} \quad (6)$$

$$Ca_3Mg(SiO_4)_2 + \text{amorphous phase} \rightarrow Ca_2SiO_4 + MgO \quad (7)$$

The presence of the mentioned transitory calcium magnesium silicate amorphous phases increases the mass transport of reactants through the sample, the limiting process of the reaction being the formation of Ca_2SiO_4.

All these reactions occur with large changes in volume. The loss of CO_2 and the large volume changes associated to reaction process disrupt the initial microstructure and create a network of new porosity (Fig. 5).

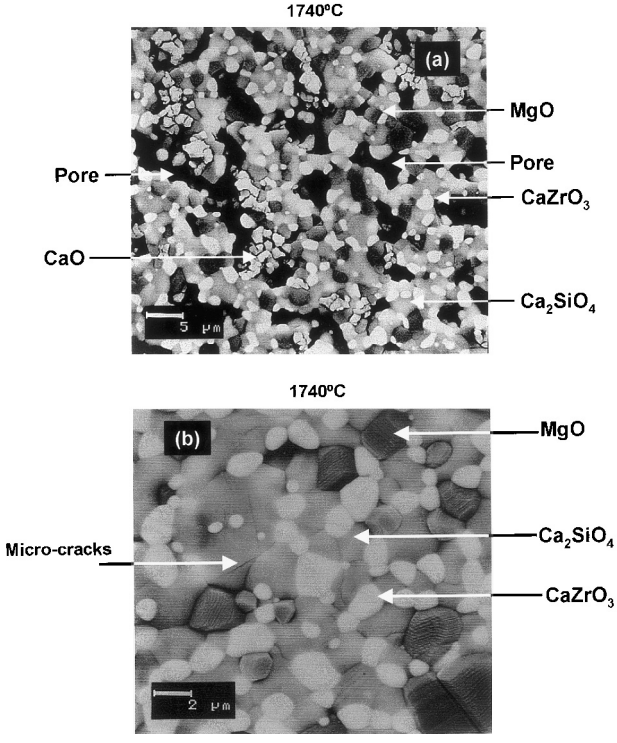

Fig. 9. Back scattered electron microscopy images of a polished and thermally etched surface of sample heat treated for 2 h at 1740°C showing: (a) general view of the sample, (b) detail of dense areas (cracks are arrowed).

The invariant point in the quaternary system $CaZrO_3 + MgO + Ca_2SiO_4$ lays at 1750°C. Hence above 1250°C the sintering occurs in solid state. Once the reaction is finished the densification begins. Within the temperature range 1250–1350°C the density of compact increases slowly.

From series of microstructures, Hg-porosimetry data and the dilatometric curves, sintering evolution can be described in the following three stages:

I. Initial stage of sintering (rearrangement and neck formation) takes place between 1250 and 1350°C. Figs. 6(a) and 7(a) and (b) show the typical microstructural

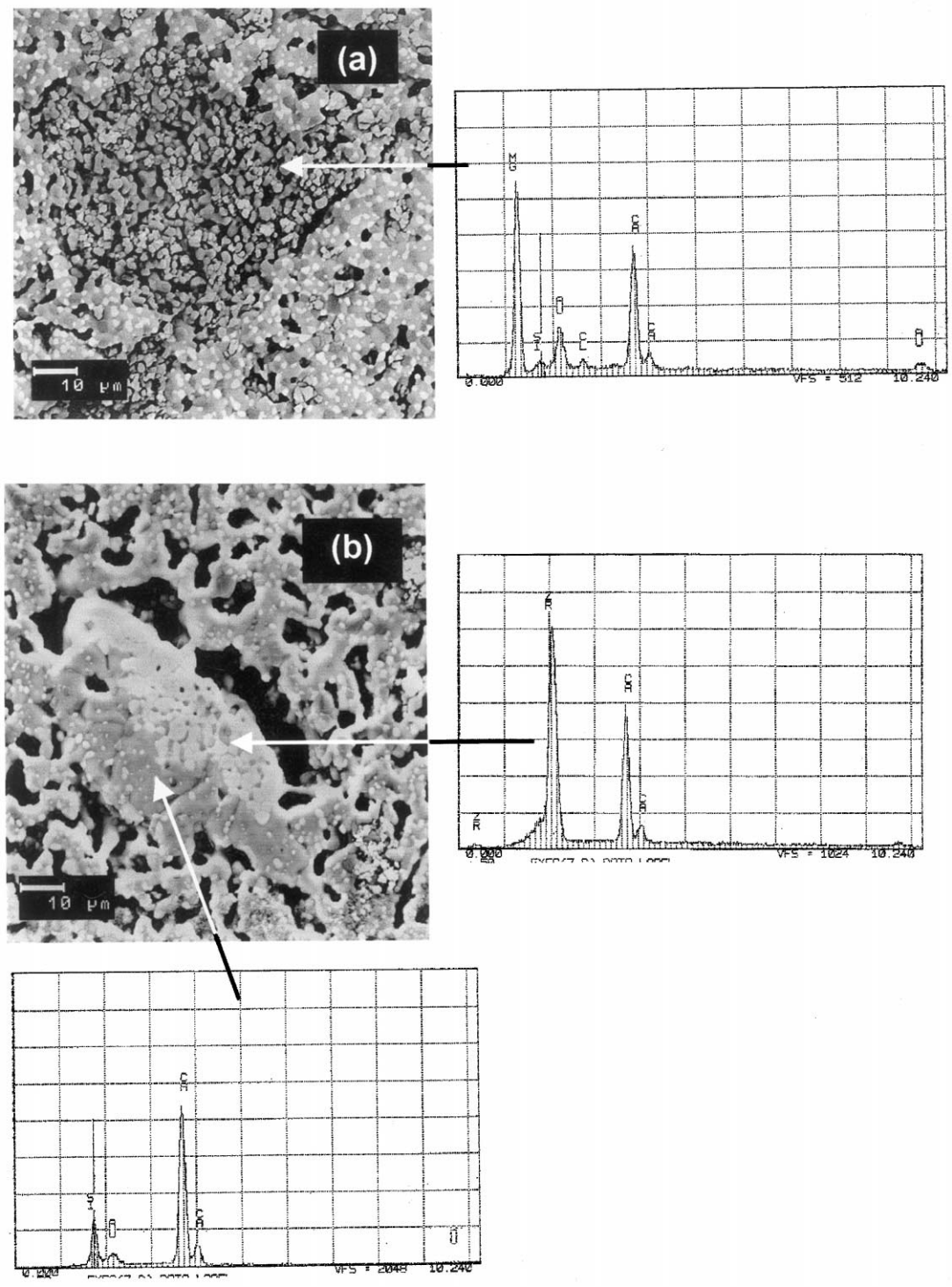

Fig. 10. (a) Micrograph showing porous biphasic clusters associated to decarbonated coarse dolomite particles. Note that magnesium and calcium ions do not diffuse. (b) Micrograph showing calcium zirconate clusters and big pores associated to coarse zircon agglomerates.

features of the sample treated at 1250°C [region I of Fig. 4(b)]. The pore size distribution of the green compact corresponds to one type of pores with an average pore size of 300 nm [Fig. 5(a)]. This pore size distribution changes significantly with temperature.

II. Intermediate stage of sintering (neck growth, grain growth, shrinkage, pore phase continuous).

The chemical reaction of reactants is practically finished at 1250°C whereas porosity is higher (61%) than the initial (25%) so no significant densification was achieved Fig. 4.

In this second stage of sintering at temperatures higher than 1550° small quantities of liquid phases are detected. These liquid phases can be due to compositional or local inhomogeneities coming from the coarse dolomite particles. The mentioned glassy phase enhances the sintering process. Both, grains and pores grow and necks between particles develop.

III. The final stage of sintering occurs in the 1600–1740°C-temperature range [region III of Fig. 4(b)]. According to the microstructural study at these temperatures the small pores are above eliminated but the density of the sample never was higher than 60%.

After sintering at temperatures as high as 1740°C the porosity of the sample is still significant (30% of theoretical). This sample shows a homogeneous microstructure with randomly distributed inhomogeneous areas Fig. 9 (a). This can be seen as areas of homogeneously distributed MgO and $CaZrO_3$ grains in the dicalcium silicate matrix [Fig. 9 (b)]. In these areas cracks can be identified. These cracks propagate along or close to $CaZrO_3$ grains and along $CaZrO_3$–Ca_2SiO_4 interfaces.

Microcracking between β-Ca_2SiO_4 and $CaZrO_3$ were often observed in $CaZrO_3$- Ca_2SiO_4 composites. Hou and Kriven first pointed it out.[11] Microcracking between Ca_2SiO_4 and $CaZrO_3$ was attributed to:

a. the thermal expansion mismatch between the different phases and
b. the polymorphs transitions of Ca_2SiO_4

However, the stress-induced beta to gamma transformation did not appear to occur in the bulk composite, since no transformation product was detected by XRD on the fracture surface.

The other significant feature of the microstructure of this sample is the clusters Figs. 9 and 10. The majority of clusters (30–60 μm) show a porous homogeneous microstructure with lime and periclase particles. The fine-grained particles of clusters sinter faster than the rest of sample, therefore, producing defects. No diffusion or reaction within the clusters and the rest of sample occurs. Similar microstructural evolution of dolomite coarse grains was observed by in situ field emission SEM observations by Suzuki et al.[12] From this type of microstructure, its clear that coarse dolomite powders decompose forming these clusters which are in equilibrium at local level and is not possible to eliminate by heat treatment. These facts inhibit the possibility of obtaining homogeneous microstructures from raw materials with medium size particles (>10 μm).

Heterogeneous $CaZrO_3/Ca_2SiO_4$ clusters (30–60 μm) surrounded by a big pore are also detected. These defects can be explained in terms of the significant differences in the diffusion rate of calcium, silica, zirconium and magnesia ions.

The segregation of large dolomite particles originates in an uneven distribution. Therefore, some small regions are richer in silica. The invariant point of compositions richer in silica in the quaternary system is located at lower temperatures. This change in the composition of one part of the sample can explain the formation of small amounts of transitory liquid phase that appears at the temperature of the invariant point $CaZrO_3 + Ca_3Mg(SiO_4)_2 + MgO + Ca_2SiO_4 +$ liq. 1550°C. This non-equilibrium situation can progress towards the corresponding equilibrium phases MgO, $CaZrO_3$ and β-Ca_2SiO_4 following the boundary $CaZrO_3 + MgO + Ca_2SiO_4 +$ Liq. to reach the invariant temperature of the ternary compatibility volume $CaZrO_3 + MgO + Ca_2SiO_4$ (1750°C, in the quaternary system).

As was described above, in this way is possible to produce high porosity materials, with a controlled microstructure, at very low cost. These characteristics open the possibility of applying them in the refractory industry as high temperature insulator. Also, due to their interconnected porosity and controlled size in the range of micrometers, these materials can be used to produce filters for liquids (industrial wastes, beverages, etc) or as membrane supports.[13]

5. Conclusions

Reaction sintering of dolomite/zircon mixtures is an inexpensive and innovative method for the synthesis of MgO–$CaZrO_3$–βCa_2SiO_4 materials.

An idealised reaction sintering mechanism, in good agreement with the experimental results, is proposed:

a. dolomite decomposition in two steps;
b. $ZrSiO_4 + \{CaO + MgO\}$ reaction with the formation of transitory amorphous silicate phases and crystallization of transitory solid phases as t-ZrO_2, $Ca_3Mg(SiO_4)_2$;
c. formation of the stable phases $CaZrO_3$, and Ca_2SiO_4 and
d. sintering of the sample.

The driving force for the solid-state reaction is much greater than the driving force for sintering at temperatures lower than 1250°C, thus the reaction precedes the densification process.

The loss of CO_2, 37% weight, and the large volume changes associated with the reaction process disrupt the initial microstructure making it possible to obtain high porous materials at temperatures as high as 1740°C.

Acknowledgements

This work was supported by CICYT, Spain, under project number MAT-97-7238. One of the authors thanks the CONACYT for the award of a fellowship.

References

1. Lee, W. E. and Rainforth, W. M., *Ceramic Microstructures. Property Control by Processing*. Chapman & Hall, London, 1994, pp. 470–488.
2. Hatfield, T., Richmond, C., Ford, W. and White, J., Relaciones de compatibilidad entre fases de periclasa y silicato en refractarios de magnesia a altas temperaturas. *Bol. Soc. Esp. Ceram. Vidrio*, 1971, **10**, 667–684.
3. Bray, D. J., Toxicity of chromium compounds formed in refractories. *Ceramic Bull*, 1985, **64**, 1012–1016.
4. Richardson, D.W., *Modern Ceramic Engineering. Properties, Processing and Use in Design*. Marcel Dekker, 1992.
5. Kriven, W. M., Possible alternative transformation toughening to zirconia: crystallographic aspects. *J. Am. Ceram. Soc.*, 1991, **71**, 1021–1030.
6. Sircar, A., Brett, N. H. and White, J., Phase studies in the system $CaO–MgO–ZrO_2–SiO_2$ Part II—Compatibility relations of zirconia. *Trans. Br. Ceram. Soc.*, 1978, **77**, 77–88.
7. De Aza, S., Richmond, C, and White, J, Compatibility relationships of periclase in the system $CaO–MgO–ZrO_2–SiO_2$. *Trans. Br. Ceram. Soc.*, 1974, **73**, 109.
8. Fullman, P. L., Measurement of particle sizes in opaque bodies. *Tans AIME*, 1953, **197**, 447–452.
9. Otsuka, R., Recent studies on the decomposition of the dolomite group by thermal analysis. *Thermochimica Acta*, 1986, **100**, 69–80.
10. De Aza, A.H., Rodriguez, M.A., Rodriguez, J.L., de Aza, S., Pena, P., and Turrilas, X., The decomposition of dolomite monitored by neutron thermodiffractometry. *Journal of the American Ceramic Society*, submitted for publication.
11. Hou, T. I. and Kriven, W. M., Mechanical properties and microstructre of $Ca_2SiO_4–CaZrO_3$ composites. *J. Am. Ceram. Soc.*, 1994, **77**, 65–72.
12. Suzuki, Y., Morgan, P., Sekino, T. and Nihihara, K., Manufacturing nano-diphasic materials from natural dolomite: in situ observation of nanophase formation behaviour. *J. Am. Ceram. Soc.*, 1997, **80**, 2949–2953.
13. Corbitt, N., *Inorganic Membranes: Markets, Technologies, Players*. Business Communications, Norwalk, 1997.